

Formation mechanism of threading-dislocation array in AlN layers grown on 6H-SiC (0001) substrates with 3-bilayer-high surface steps

Hironori Okumura, Tsunenobu Kimoto, and Jun Suda

Citation: [Applied Physics Letters](#) **105**, 071603 (2014); doi: 10.1063/1.4892807

View online: <http://dx.doi.org/10.1063/1.4892807>

View Table of Contents: <http://scitation.aip.org/content/aip/journal/apl/105/7?ver=pdfcov>

Published by the [AIP Publishing](#)

Articles you may be interested in

[In-situ NC-AFM measurements of high quality AlN\(0001\) layers grown at low growth rate on 4H-SiC\(0001\) and Si\(111\) substrates using ammonia molecular beam epitaxy](#)

[AIP Advances](#) **5**, 067108 (2015); 10.1063/1.4922193

[Studies of the annihilation mechanism of threading dislocation in AlN films grown on vicinal sapphire \(0001\) substrates using transmission electron microscopy](#)

[Appl. Phys. Lett.](#) **87**, 101910 (2005); 10.1063/1.2042533

[On the microstructure of Al_xGa_{1-x}N layers grown on 6H-SiC\(0001\) substrates](#)

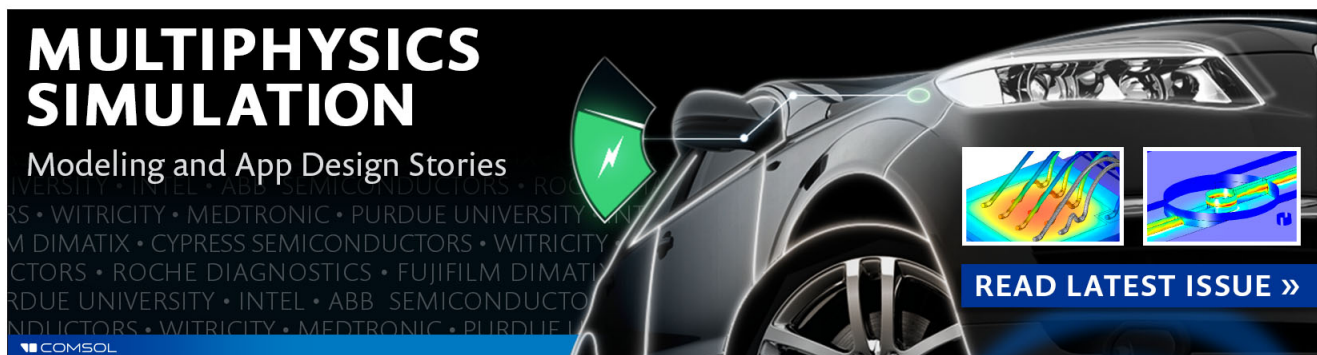
[J. Appl. Phys.](#) **97**, 083501 (2005); 10.1063/1.1861152

[Nucleation and growth kinetics of AlN films on atomically smooth 6H-SiC \(0001\) surfaces](#)

[Appl. Phys. Lett.](#) **78**, 3612 (2001); 10.1063/1.1377309

[Influence of 6H-SiC\(0001\) substrate surface morphology on the growth of AlN epitaxial layers](#)

[Appl. Phys. Lett.](#) **74**, 985 (1999); 10.1063/1.123431

The advertisement features a dark background with a sleek, modern car on the right side. On the left, the text 'MULTIPHYSICS SIMULATION' is written in large, bold, white capital letters. Below it, 'Modeling and App Design Stories' is written in a smaller white font. A green lightning bolt icon is positioned to the left of the car. Two small inset images show colorful simulation results: one with blue and yellow gradients, and another with a blue and red gradient. At the bottom right, a blue button with white text says 'READ LATEST ISSUE >>'. The COMSOL logo is visible in the bottom left corner.

**MULTIPHYSICS
SIMULATION**
Modeling and App Design Stories

READ LATEST ISSUE >>

COMSOL

Formation mechanism of threading-dislocation array in AlN layers grown on 6H-SiC (0001) substrates with 3-bilayer-high surface steps

Hironori Okumura,^{1,a)} Tsunenobu Kimoto,^{1,2} and Jun Suda¹

¹Department of Electronics Science and Engineering, Kyoto University, Kyoto 615-8510, Japan

²Photonics and Electronics Science and Engineering Center, Kyoto University, Kyoto 615-8510, Japan

(Received 21 June 2014; accepted 23 July 2014; published online 19 August 2014)

We grew AlN layers on 6H-SiC (0001) substrates with three Si-C bilayer high (0.75 nm) steps. In the AlN layers, most of the threading dislocations (TDs) were arranged in rows. The TD row consisted of arrays of a half-loop dislocation, which was formed by an AlN/SiC interfacial dislocation along the step edges of the SiC substrate surfaces and a TD pair at both ends. The configuration of the interfacial dislocation was highly relevant with two-dimensional AlN nuclei at the initial stage of growth. We concluded that the half-loop dislocation arrays were generated in the AlN nucleus coalescence over the SiC step edges. © 2014 AIP Publishing LLC.

[<http://dx.doi.org/10.1063/1.4892807>]

AlN is one of the most promising materials for deep-UV light-emitting diodes (LEDs) and high-temperature electronics devices due to its large band-gap energy (6.1 eV). AlN LEDs with an emission wavelength of 205 nm allow downsizing and less power consumption than traditional techniques using mercury lamps. However, AlN LEDs have not been in practical use due to low external quantum efficiency (EQE).^{1,2} One factor in the low EQE is the non-radiative recombination center due to threading dislocations (TDs).³ AlN is usually grown on foreign substrates because of the small size and the high cost of AlN bulk crystals. The TD density (TDD) in typical AlN epilayers is very high ($\sim 10^{10} \text{ cm}^{-2}$). A growth technique of AlN hetero-epitaxial layers with a low defect density must be established to increase the EQE of AlN LEDs.

For AlN (0001) epitaxial growth, SiC (0001) is one of the most suitable substrates due to the small lattice mismatch (1%) between AlN and SiC, the same hexagonal structure as AlN, and commercially available high-quality large-area (up to 6 in.) SiC wafers. However, AlN growth on SiC substrates has two critical issues: polytype and valency mismatches.⁴ These issues contribute to the high density of TDs and threading planar defects, which are generated at AlN/SiC interfaces and extend through the AlN layers.^{5–8} Therefore, we must overcome these two issues and reduce the density of TDs and the planar defects.

AlN has a different stacking sequence (polytype) from SiC; it has a wurzite (2H) structure (Al-N bilayer stacking sequence of AB...), and a typical SiC has a 4H (ABCB...) or 6H (ABCACB...) structure. Owing to the polytype mismatch, 2H-AlN grown on 4H- or 6H-SiC (0001) substrates has different stacking arrangements on each terrace and yields threading planar defects, which are called stacking mismatch boundaries (SMBs), over the step edges of the SiC substrate surfaces.^{9–11} SiC substrates with controlled step heights¹² or with step-free surfaces¹³ are effective to avoid generating SMBs in the AlN growth. We adopted the step-height control method in which the intended surfaces are uniformly obtained at a large area.

If SiC's step height is controlled by the unit cell (6 bilayers for 6H-SiC and 4 bilayers for 4H-SiC), the AlN stacking arrangements on each (0001) terrace of SiC correspond without generating SMBs. Unit-cell-high steps can be formed by a micro-step bunching phenomenon during high-temperature gas etching^{14,15} or SiC homoepitaxial growth.¹⁶ We obtained 6-bilayer-high steps by the high-temperature H₂-gas etching of 6H-SiC (0001) substrates, but the area was limited to several mm² due to the slight fluctuation in the off-direction from $\langle 1\bar{1}00 \rangle$.¹¹ We uniformly obtained half-unit-cell (3-bilayer) steps at a whole 2-in. 6H-SiC wafer due to an insensitive off-direction and found that 6H-SiC substrates with 3-bilayer-high steps as well as 6-bilayer-high steps enable AlN growth without SMBs.^{11,17} In practical terms, we used 6H-SiC (0001) substrates with 3-bilayer-high steps for AlN growth without SMBs.

AlN is a III–V compound semiconductor, but SiC is a IV–IV compound semiconductor. This valency mismatch increases the interface energy between AlN and SiC and contributes to the three-dimensional (3D) growth mode at an initial growth stage of AlN growth on SiC.^{18,19} The 3D growth mode, which has a deformed lattice spacing to reduce the elastic-strain energy, causes a high density of dislocations in the 3D islands²⁰ and the 3D island coalescence.²¹ By using metal gallium (Ga) as a surfactant and immediately starting the AlN growth after the nitrogen plasma was ignited, we achieved a two-dimensional (layer-by-layer) growth mode just after the AlN growth.^{17,22,23} A 300-nm-thick AlN layer, which was coherently grown on SiC,^{24,25} successfully reduced the TDD to $4 \times 10^8 \text{ cm}^{-2}$. Our transmission electron microscopy (TEM) studies revealed that most of the TDs in the AlN layer on the 6H-SiC substrates with 3-bilayer-high steps were arranged in rows.^{11,17} In this study, we clarified the generation mechanism of the TD rows by focusing on the defect structure in the AlN layers on 6H-SiC (0001) substrates with 3-bilayer-high steps to obtain clues for further TDD reduction.

We used 6H-SiC (0001) (vicinal angle of 0.2° toward $10 \pm 2^\circ$ from $[1\bar{1}00]$ to $[21\bar{1}0]$) semi-insulating substrates treated with chemical mechanical polishing (CMP). By high-temperature H₂-gas etching in a hot-wall chemical-vapor

^{a)}E-mail: okumura@semicon.kuee.kyoto-u.ac.jp

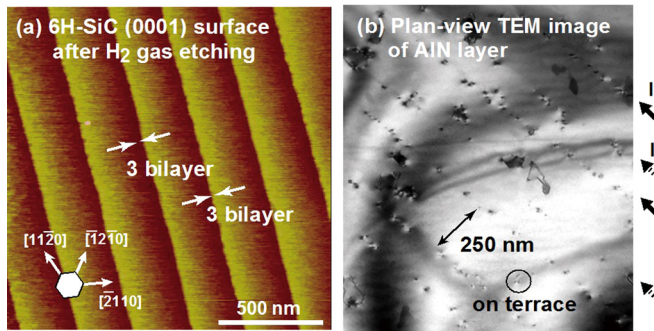


FIG. 1. (a) Surface morphology of 6H-SiC (0001) after high-temperature H_2 -gas etching. 3-bilayer-high steps (0.75 nm) and atomically smooth terrace with widths of 200–300 nm were obtained. (b) Bright-field plan-view TEM image (zone axis) of 300-nm-thick AlN layer on 6H-SiC (0001) with 3-bilayer-high steps. TDs are arranged in rows, indicated by arrows. Separation of TD rows is between 200 and 300 nm. TD rows are generated over step edges of SiC and have two types of defect structures I and II.

deposition (CVD) system, the SiC step height was controlled to three bilayers (0.75 nm).¹² The surface morphology of the gas-etched 6H-SiC (0001) substrate is shown in Fig. 1(a). It had a step-and-terrace structure with 3-bilayer-high steps (0.75 nm). We obtained atomically smooth terraces and sharp step edges (facet angles are thought to exceed 12° , Ref. 26). Just before the AlN growth, each substrate was cleaned by an *ex situ* wet process, loaded into the exchange chamber of a plasma-assisted molecular-beam epitaxy (PAMBE) system, heated at around 200°C for degassing, and loaded into the main chamber. The MBE system is equipped with effusion cells for Ga and Al evaporation and a Veeco Unibulb radio-frequency (rf) plasma cell for producing active nitrogen. The residual oxygen adsorbed on the substrates was removed by *in situ* Ga deposition and desorption processes.⁵ The SiC substrate was exposed to 2 monolayers (ML) of metal Ga as soon as the nitrogen plasma was ignited.¹⁷ Next, AlN was grown at 650°C at 5 nm/min under Al-rich conditions. The layer-by-layer growth mode from a very early stage of growth was confirmed by reflective high-energy electron diffraction (RHEED) intensity oscillations. After 300-nm-thick growth, the AlN surfaces had a step-and-terrace structure with 1-bilayer-high steps (0.25 nm). The surface morphologies and defect structures of the AlN layers were evaluated by atomic force microscopy (AFM) (Veeco D-3100) and TEM (JEOL JEM-2100F), respectively.

In cross-sectional TEM observation (not shown), most of the TDs (>99%) were invisible at the two-beam conditions of diffraction vector $\mathbf{g} = 0001$, while the TDs had a weak contrast at the two-beam conditions of $\mathbf{g} = 1\bar{1}00$, indicating a pure-edge type (Burgers vector $\mathbf{b} = 1/3\langle 11\bar{2}0 \rangle$). All of the observed TDs were basically extended normally (85° – 90°) to the AlN surface from the AlN/SiC interface. The slight TD inclination ($<5^\circ$) was attributed to a compressive strain in the AlN/SiC hetero-epitaxial growth.²⁷

A bright-field plan-view TEM image (zone axis) of a 300-nm-thick AlN layer is shown in Fig. 1(b). TDs are observed as dark spots. Most are arranged in rows with separation widths of 200–300 nm. Their separation widths of the TD rows correspond to the (0001) terrace widths of the SiC substrate before the growth (Fig. 1(a)), indicating that the TD rows were generated over the step edges of the SiC

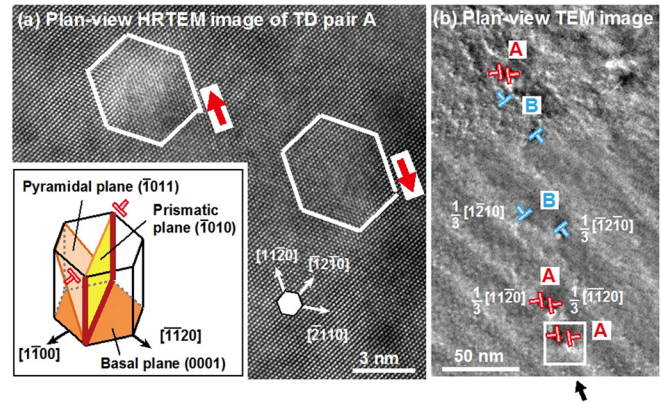


FIG. 2. (a) Plan-view HRTEM image of TD pair A in AlN layer and magnified image of white square in Fig. 2(b). Relation between slip planes $\{1\bar{1}00\}$ and TD pairs is schematically shown in the inset figure. (b) Bright-field plan-view TEM image of TD row in 100-nm-thick AlN layer on 6H-SiC (0001) with 3-bilayer-high steps. There are two types of TD pairs (A and B) with different Burgers vectors.

surface. The TDD in the TD rows was $3 \times 10^9 \text{ cm}^{-2}$, which was one order of magnitude higher than the density ($4 \times 10^8 \text{ cm}^{-2}$) of the TDs generated on the terraces of the SiC surface (circle in Fig. 1(b)). These results suggest that the pure-edge type TDs generated over the SiC step edges are the most critical issue to reduce TDDs in the AlN layer. Detailed investigation of Fig. 1(b) distinguishes TD rows with two types of low and high TDD. In this paper, TD rows I and II is our name for the TD rows with low and high TDDs, respectively, which were alternatively observed.

A plan-view high-resolution (HR) TEM image of two TDs in the TD row II for a 100-nm-thick AlN layer is shown in Fig. 2(a). The Burgers vectors of the two TDs faced opposite directions: $\mathbf{b} = 1/3[11\bar{2}0]$ and $1/3[\bar{1}\bar{1}20]$. Fig. 2(b) shows a plan-view TEM image of ten TDs, which include the above two TDs. All ten TDs in TD row II had Burgers vectors of an edge-type component, consisting of cross-sectional TEM observation at two beam conditions. These ten TDs can be separated into five sets of TD pairs with Burgers vectors of opposite directions. For the TD row I (not shown), two TDs also had Burgers vectors of opposite directions. These results indicate that the TD rows consist of dislocation pairs. In Fig. 2(b), the five TD pairs in TD row II can be separated into the following two types: pair A with $\mathbf{b} = 1/3[11\bar{2}0]$ and $1/3[\bar{1}\bar{1}20]$ and pair B with $\mathbf{b} = 1/3[1\bar{2}10]$ and $1/3[\bar{1}2\bar{1}0]$. Another TD pair with \mathbf{b} of $1/3[2\bar{1}10]$ and $1/3[2\bar{1}\bar{1}0]$, which is nearly parallel to the off-direction $[21\bar{1}0]$ of the substrate surface, was not observed.

A plan-view TEM image of a 50-nm-thick AlN layer at a 20° tilt is shown in Fig. 3(a) and includes the SiC substrate and the AlN layer because the TEM specimen's thickness exceeds 50 nm. Dark lines parallel to the AlN/SiC interface were observed at the same position as the TD rows. A dark line and two TDs consisted of a U-shaped structure, i.e., half-loop defects (Fig. 3(b)), which were arranged in rows without overlapping. These indicate that the TD rows consist of dislocation half-loop arrays, agreeing with the observation of the dislocation pairs in Fig. 2(a). Under two beam conditions, we confirmed that the dark lines (interfacial dislocations) had Burgers vectors with $\langle 11\bar{2}0 \rangle$ directions. We

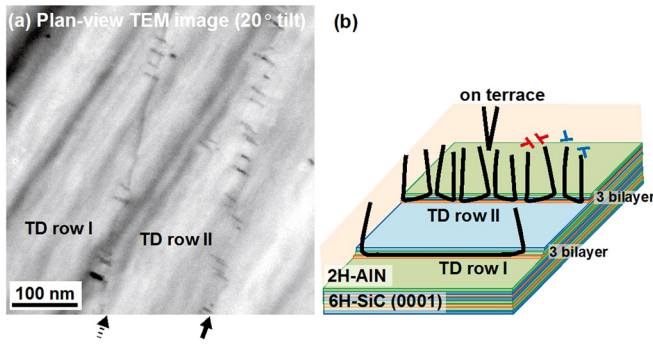


FIG. 3. (a) Bright-field plan-view TEM image (20° tilt) of 50-nm-thick AlN layer on 6H-SiC (0001) with 3-bilayer-high steps. This image includes the SiC substrate; no defects were observed in it due to the high quality (TDD less than 10^4 cm^{-2}). (b) Schematic image of TD rows in AlN layer on 6H-SiC with 3-bilayer-high steps. TDs over SiC step edges have a U-shaped structure, and those on SiC terraces have a V-shaped structure.

consider that the interfacial dislocations over the SiC step edges are misfit dislocations due to the lattice mismatch (1%) between AlN and SiC.

The misfit-dislocation line direction was near $\langle 11\bar{2}0 \rangle$ and made a 60° angle with the Burgers vector, corresponding to other reports.²⁸ For a triangular misfit dislocation array, plastic relaxation ε is given by $\varepsilon = 3/2 \cdot (b_e \sin\beta) / l$, where b_e is the magnitude for edge component of the Burgers vector, β is the angle between the misfit dislocation line and the Burgers vector, and l is the misfit dislocation spacing.²⁷ By assuming that the lattice of an AlN layer over the step edges of the SiC substrates (terrace width l of 300 nm) is just relaxed toward the $[\bar{2}110]$ direction, effective plastic relaxation $\varepsilon' = 1/3\varepsilon = 0.045\%$, which is much smaller than the 1% lattice difference between AlN and SiC. Next, we estimated the residual in-plane strain (ε_{xx}) in the AlN layer at 9.62×10^{-3} , corresponding to the value ($\varepsilon_{xx} = 9.62 \times 10^{-3}$) calculated from the 2θ - ω X-ray diffraction (XRD) scans in the symmetric (0002) reflection of the 300-nm-thick AlN layer grown on SiC.²¹ We consider that the AlN layers just over the SiC step edges were slightly relaxed, causing TD arrays with misfit dislocations.

Detailed TEM observation (Fig. 3(a)) shows two types of TD rows with different dislocation density, corresponding to TD rows I and II in Fig. 1(b). TD row I (low TDD) is on a straight line and has long dark lines (~ 100 nm), and TD row II (high TDD) has a zigzag structure with short dark lines (~ 30 nm). These two types of TD rows were alternatively observed. We noticed that the structures of the TD rows resembled the surface morphology of an AlN layer at an initial growth stage (Fig. 4(a)). Until around-10-nm AlN growth, 3-bilayer-high steps were maintained on the AlN surface²³ and 2D nuclei were observed on the SiC terraces. Due to the threefold symmetry of the AlN crystal, the AlN 2D nucleus has a triangular shape with $\{1\bar{1}00\}$ facets, like GaN.²⁹ Triangle 2D nuclei are inverted on each terrace of the SiC surfaces because the stacking arrangements of the AlN layer on 6H-SiC with an odd number of 3-bilayer-high steps are different on each terrace.¹² We alternatively observed two types of step-edge shapes of AlN surfaces, i.e., straight and zigzag. These AlN 2D nuclei had similar shapes to the misfit dislocations generated over the SiC step edges, suggesting that the AlN nuclei coalescence over the SiC step

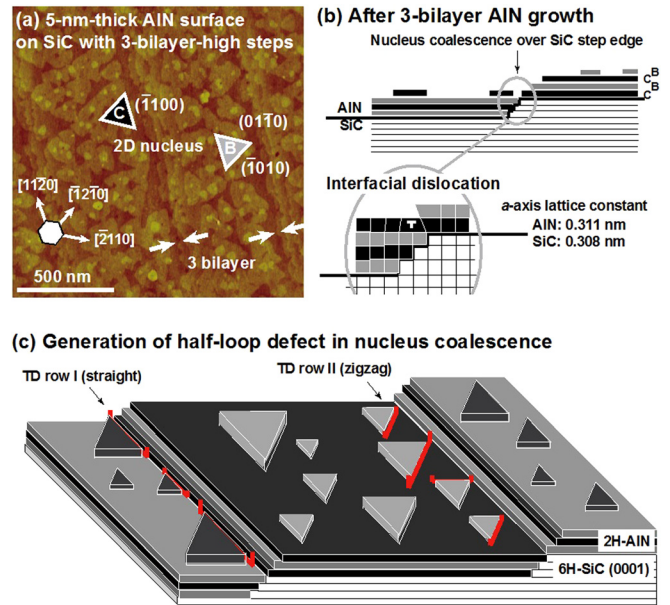


FIG. 4. (a) Surface morphology of 5-nm-thick AlN layer on 6H-SiC (0001) with 3-bilayer-high steps. AlN has a layer-by-layer growth mode. Triangle-shaped 2D nuclei of AlN are observed because of a three-fold symmetry. (b) and (c) Schematic images of generation mechanism of interfacial dislocations in AlN layer on 6H-SiC (0001) with 3-bilayer-high steps. Interfacial dislocations are generated over step edges of the SiC substrate to reduce the tensile strain in nucleus coalescence after 3-bilayer AlN growth.

edges reflects the generation of the misfit dislocations in the TD rows.

We discuss the origin of the misfit dislocations over the step edges of 6H-SiC (0001) with 3-bilayer-high steps. A lattice-mismatch film accumulates in-plane strain energy during growth, and its overly critical thickness causes lattice relaxation by introducing misfit dislocations. In this work, the AlN epilayer was coherently grown on SiC terraces in a layer-by-layer growth mode and only caused misfit dislocations over the step edges of the SiC substrates, indicating that few misfit dislocations result from the glide motions of pre-existing or new dislocations that should be randomly distributed. Massies and Grandjean reported that misfit dislocations can be generated in the nucleus coalescence because the compressive/tensile strain energy in the epilayer expands outward/inward in the lattice spacing near the nucleus edges.³⁰ In AlN coherently grown on SiC, a compressive strain must exist because of a larger a -axis lattice constant of AlN (0.311 nm) than SiC (0.308 nm) that expands outward in the lattice spacing near the AlN nucleus edges. Each strained AlN nucleus on the adjacent terraces coalesces over the SiC step edges after the 3-bilayer AlN growth (Fig. 4(b)). The deletion of a prismatic plane between the coalesced AlN nuclei yielded a $\langle 11\bar{2}0 \rangle$ misfit dislocation over the SiC step edges to relieve part of the in-plane strain energy in the 0.75-nm-thick AlN layer.

Based on the above discussion (Fig. 4(b)), misfit dislocation is generated between a $\{1\bar{1}00\}$ facet of an AlN 2D nucleus and a step edge of the AlN surface. If an AlN 2D nucleus perfectly coalesces with the AlN step edges without an extra-half plane (Fig. 4(c)), the misfit dislocation bends at the coalesced point and extends to the surface, generating half-loop dislocation with a dislocation pair. In the layer-by-layer growth mode, two types of AlN nuclei alternatively

appeared on the adjacent SiC terraces due to threefold symmetry (Fig. 4(a)), which resembled the structure of the TD rows (Fig. 3(b)). From these results, we propose that the misfit dislocations bend at some changing points of the $\{1\bar{1}00\}$ facets of AlN 2D nuclei, e.g., a point between the $(01\bar{1}0)$ and $(\bar{1}010)$ facets, causing dislocation half-loop arrays. In this model, the 2D nuclei with straight step edges, which face only a $(1\bar{1}00)$ facet for 3-bilayer-high AlN steps (black triangles in Fig. 4(a)), generate long misfit dislocations (~ 100 nm), resulting in TD row I (low TDD). The 2D nuclei with zigzag step edges, which face both $(01\bar{1}0)$ and $(\bar{1}010)$ facets (gray triangles in Fig. 4(a)), yield many short misfit dislocations (~ 10 nm), resulting in TD row II (high TDD). If we can control the AlN nuclei coalescence over the SiC step edges, further reduction of the TD rows will be possible.

In summary, we have reported a generation mechanism of half-loop dislocation arrays in AlN layers on 6H-SiC substrates with 3-bilayer-high steps. Most of the TDs were formed over the SiC step edges and consisted of half-loop dislocation arrays, including a misfit dislocation along the SiC step edge at the AlN/SiC interface and a TD pair at the both ends. We concluded that the dislocation arrays were generated in the AlN nuclei coalescence to relieve the in-plane stress due to a lattice mismatch between AlN and SiC.

This work was supported by the Global Center of Excellence (COE) Program (C09) from the Ministry of Education, Culture, Sports, Science and Technology of Japan as well as a Grant-in-Aid from the Japan Society for the Promotion of Science (21.5229).

¹Y. Taniyasu, M. Kasu, and T. Makimoto, *Nature* **441**, 325 (2006).

²J. R. Grandusky, S. R. Gibb, M. C. Mendrick, C. Moe, M. Wraback, and L. J. Schowalter, *Appl. Phys. Express* **4**, 082101 (2011).

³H. Amano, A. Miyazaki, K. Iida, T. Kawashima, M. Iwaya, S. Kamiyama, I. Akasaki, R. Liu, A. Bell, F. A. Ponce, S. Sahonta, and D. Cherns, *Phys. Status Solidi A* **201**, 2679 (2004).

⁴L. Liu and J. H. Edgar, *Mater. Sci. Eng.* **37**, 61 (2002).

⁵N. Onojima, J. Suda, and H. Matsunami, *Jpn. J. Appl. Phys., Part 2* **42**, L445 (2003).

⁶Y. Taniyasu, M. Kasu, and T. Makimoto, *J. Cryst. Growth* **298**, 310 (2007).

⁷M. Imura, H. Sugimura, N. Okada, M. Iwaya, S. Kamiyama, H. Amano, I. Akasaki, and A. Bandoh, *J. Cryst. Growth* **310**, 2308 (2008).

⁸A. Kakanakova-Georgieva, D. Nilsson, and E. Janzen, *J. Cryst. Growth* **338**, 52 (2012).

⁹C. Drum, *Philos. Mag.* **11**, 313 (1965).

¹⁰S. Tanaka, R. S. Kern, and R. F. Davis, *Appl. Phys. Lett.* **66**, 37 (1995).

¹¹H. Okumura, M. Horita, T. Kimoto, and J. Suda, *Phys. Status Solidi A* **206**, 1187 (2009).

¹²H. Okumura, M. Horita, J. Suda, and T. Kimoto, *Appl. Surf. Sci.* **254**, 7858 (2008).

¹³N. D. Bassim, M. E. Twigg, M. A. Mastro, C. R. Eddy, T. J. Zega, R. L. Henry, J. C. Culbertson, R. T. Holm, P. Neudeck, J. A. Powell, and A. J. Trunek, *J. Cryst. Growth* **304**, 103 (2007).

¹⁴C. Hallin, F. Owman, P. Martensson, A. Ellison, A. Konstantinov, O. Kordina, and E. Janzen, *J. Cryst. Growth* **181**, 241 (1997).

¹⁵S. Nakamura, T. Kimoto, and H. Matsunami, *Appl. Phys. Lett.* **76**, 3412 (2000).

¹⁶T. Kimoto, A. Itoh, H. Matsunami, and T. Okano, *J. Appl. Phys.* **81**, 3494 (1997).

¹⁷H. Okumura, T. Kimoto, and J. Suda, *Appl. Phys. Express* **4**, 025502 (2011).

¹⁸D. G. Ebling, M. Rattunde, L. Steinke, K. W. Benz, and A. Winnacker, *J. Cryst. Growth* **201–202**, 411 (1999).

¹⁹N. Teraguchi, A. Suzuki, Y. Saito, T. Yamaguchi, T. Araki, and Y. Nanishi, *J. Cryst. Growth* **230**, 392 (2001).

²⁰R. V. Kukta and L. B. Freund, *J. Mech. Phys. Solids* **45**, 1835 (1997).

²¹N. Onojima, J. Suda, and H. Matsunami, *J. Cryst. Growth* **237–239**, 1012 (2002).

²²G. Mula, C. Adelman, S. Moehl, J. Oullier, and B. Daudin, *Phys. Rev. B* **64**, 195406 (2001).

²³H. Okumura, T. Kimoto, and J. Suda, *Phys. Status Solidi C* **7**, 2094 (2010).

²⁴H. Okumura, T. Kimoto, and J. Suda, *Appl. Phys. Express* **5**, 105502 (2012).

²⁵M. Kaneko, H. Okumura, R. Ishii, M. Funato, Y. Kawakami, T. Kimoto, and J. Suda, *Appl. Phys. Express* **6**, 062604 (2013).

²⁶H. Nakagawa, S. Tanaka, and I. Suemune, *Phys. Rev. Lett.* **91**, 226107 (2003).

²⁷B. Moran, F. Wu, A. E. Romanov, U. K. Mishra, S. P. Denbaars, and J. S. Speck, *J. Cryst. Growth* **273**, 38 (2004).

²⁸J. Bai, X. Huang, and M. Dudley, *Mater. Sci. Semicond. Process.* **9**, 180 (2006).

²⁹M. H. Xie, S. M. Seutter, W. K. Zhu, L. X. Zheng, H. Wu, and S. Y. Tong, *Phys. Rev. Lett.* **82**, 2749 (1999).

³⁰J. Massies and N. Grandjean, *Phys. Rev. Lett.* **71**, 1411 (1993).